Mechanisms of ethidium bromide removal by Ca-montmorillonite

Po-Hsiang Chang[a], Zhaohui Li[b,*], Wei-Teh Jiang[c,*]

[a]School of Human Settlements and Civil Engineering, Xi'an Jiaotong University, 28 Xianning West Road, Xi'an, Shaanxi, 710049, P.R. China, email: tectonicion@xjtu.edu.cn
[b]Department of Geosciences, University of Wisconsin – Parkside, Kenosha, WI 53144, USA, email: li@uwp.edu
[c]Department of Earth Sciences, National Cheng Kung University, Tainan 70101, Taiwan, email: atwtj@mail.ncku.edu.tw

ABSTRACT

Ethidium bromide is extensively used in many biochemical laboratories. Due to its high toxicity, its removal from the wastewater before being disposed becoming an emerging issue. Swelling clay minerals, due to their inexpensive material cost, high efficiency, and vast reserves, have been evaluated for the removal of different types of contaminants. In this study, the removal of ethidium bromide, particularly its mechanism of removal was assessed, using Ca-montmorillonite (SAz-1) as a representative swelling clay minerals. The ethidium bromide removal could reach equilibrium within 1 h and a capacity of 1,276 mmol kg^{-1}, same magnitude as the cation exchange capacity of SAz-1. The total amount of metal cations desorbed from SAz-1 to the amount of ethidium removed was linearly correlated with a slope of 0.7, suggesting cation exchange as the dominant mechanism. In addition, the less-than-unity desorption/adsorption ratio could be attributed to the removal of ethidium dimers bridged with bromide counterions. An increase of the basal spacing to 18.3 Å for SAz-1 after adsorption implied that intercalation of flat-lying ethidium dimers into the clay interlayer, which increased its thermal stability, and active participation of the amine groups of ethidium molecules in the adsorptive interaction was evidenced from Fourier transform infrared band shifts. The results suggested that Ca-montmorillonite is an excellent candidate for fast and effective removal of ethidium bromide from aqueous solution. As such, it could serve as an ideal packing material for kits to be manufactured and used for ethidium bromide removal in case of spill.

Keywords: Ethidium bromide; Montmorillonite; Adsorptive removal; Desorption

1. Introduction

Ethidium bromide, 3,8-diamino-6-phenyl-5-ethyl-phenanthridine bromide is an aromatic compound with a tricyclic structure having aniline groups on two sides of a pyridine moiety (Fig. S1). The cyclic groups of ethidium bromide are hydrophobic, similar to the aromatic rings of DNA bases. Ethidium bromide is commonly used as a marker for labeling nucleic acid bands in electrophoresis as well as other methods of nucleic acid separation. Because of the widespread practice of single cell gel electrophoresis assay, some excess fractions of ethidium bromide may leave research laboratories and reside in the environment, and like most of other nucleic acid fluorescent dyes, ethidium bromide has high toxicity and carcinogenicity to human cells [1–3]. Furthermore, toxic effects on agriculturally important crops such as wheat, alfalfa, and tomato due to irrigation with ethidium bromide-containing water were reported [4], calling for a broad watch on the impact and attenuation of ethidium bromide in aqueous environments. As such, exploring effective materials and

*Corresponding authors.

mechanisms for its removal is an important task in pertinent laboratories as well as treatment plants.

Adsorption is one of the most effective removal methods for a large number of different contaminants. Adsorbents such as graphene oxide [5], pumice [6], CuO nanoparticles [7], carboxylate group functionalized and unmodified single-walled carbon nanotube [8], acid washed kaolinite and alumina [9], and nano-scale zero-valent iron [10] were used to remove ethidium bromide from aqueous solutions (Table S1). Most of the above adsorbents require a preparation protocol involving uses of harsh chemical reagents (e.g., heavy metals for nanoparticle synthesis and borohydride for zero-valence iron synthesis) that could raise concerns about potential secondary pollution in working applications. Moreover, the production of nano-sized adsorbents (e.g., carbon nanotubes) may require high energy consumption with high costs in various aspects and have applications limited in specific areas in practice.

In contrast, naturally occurring expandable clays, particularly smectitic minerals are known to be highly efficient for adsorptive removal of various contaminants at low cost. Studies using pristine or modified clay minerals to remove single and multiple contaminants from water were conducted extensively in the past [11,12]. However, tests for the removal of ethidium bromide by clays are limited. Rectorite, a regularly mixed-layer illite/smectite clay was able to remove ethidium bromide from aqueous solution in a fast adsorption process, reaching an adsorption capacity as high as 160 mg g^{-1} equivalent to the cation exchange capacity (CEC) of the clay [13]. Cation exchange was determined to be the key mechanism for the adsorption but the amount of desorbed cations was only about a half of the amount of ethidium cations adsorbed on the rectorite [13].

Montmorillonite as a dioctahedral smectite is characterized by high values of CEC and specific surface area (SSA). As such, it could absorb the ethidium bromide via conceivable cation exchange mechanism. Furthermore, montmorillonite has the characteristics of abundant, cheap and easy to obtain, so it could not only realize the use of low-cost materials to show (1) high economy and practicality; (2) rapid adsorption; (3) high adsorption effect for multiple purposes, and it can be used in industry or household. The wastewater treatment process can achieve (1) zero greenhouse gas emissions; (2) no heat generation on the environment; (3) no secondary pollution during adsorption. Under these scenarios, the clay mineral has the very astonishing advantage to absorb the organic compound such as ethidium bromide.

Uptake of ethidium bromide by Na-montmorillonite (SWy-2) and Ca-montmorillonite (SAz-2 and STx-1b) from aqueous solution could reach an adsorption capacity up to 600 mg g^{-1} and the clays could be regenerated by heating to 500°C [14]. However, mechanisms for the uptake of ethidium bromide by those montmorillonites were not elucidated. As such, further exploration of the potential application of using montmorillonites for ethidium bromide removal could be hindered.

This study focused on systematic analyses of the interactions between Ca-montmorillonite and ethidium bromide using thermogravimetric, X-ray diffraction, and Fourier transform infrared spectroscopy (FTIR) analyses, in conjunction with the desorption of exchangeable cations in association with ethidium bromide removal, so that the mechanisms of ethidium bromide removal could be elucidated.

2. Materials and methods

2.1. Materials

Ethidium bromide ($C_{21}H_{20}BrN_3$, CAS No. 1239-45-8) has a molecular weight of 394.3 g mol^{-1} and a water solubility of 40 g L^{-1}. When dissolved in water, it may form a cation ethidium$^+$ and its two amine groups can be protonated at pH 2.43 (pK_{a2}) and 0.71 (pK_{a1}) [15]. It has a molecular dimension of 10.0 × 11.0 × 5.0 Å computed by the ChemSketch Software (Fig. S1). The Ca-montmorillonite SAz-1 (from the Source Clays Repository of the Clay Minerals Society) was used without further purification. It contains ~98% montmorillonite, ~1% quartz, and ~1% other minerals by X-ray diffraction analyses [16]. The reported CEC and SSA values were 1,230 meq kg^{-1} and 65 m^2 g^{-1}, respectively [17]. The total surface area of SAz-1 including the external surface and interlayer areas was 736 m^2 g^{-1}, suggesting that the montmorillonite particles may be made of stacking about 10 unit cells along the *c* crystallographic direction [18].

2.2. Batch adsorption experiments

To each 50 mL centrifuge tube, 0.1 g of SAz-1 and 20 mL of ethidium bromide solution were added. All tubes were wrapped with aluminum foils to prevent possible light-induced decomposition of the compound. For all experiments, except the isotherm study, the initial ethidium bromide concentration was 8 mmol L^{-1}. The final solution pH values were close to 7 without pH adjustment, aside from those for the pH-dependent study. For the kinetic study, the mixing time was 0.25, 0.5, 1.0, 2.0, 4.0, 8.0, 16.0 and 24.0 h. For the pH-dependent test, the equilibrium solution pH was checked periodically and adjusted to between 2 and 11 by dropwise addition of 2 M NaOH or 2 M HCl to minimize the change in total liquid volume. For the ionic strength study, NaCl and CaCl$_2$ were used as the ionic strength tuners at concentrations of 0.001, 0.01, 0.1, and 1.0 M. For the temperature-dependent analysis, the temperature was maintained at 303, 318, and 333 K. For the adsorption isotherm study, the initial ethidium bromide concentrations were 2, 4, 6, 8, 10, 12, and 14 mmol L^{-1}. The mixtures were swayed on a reciprocal shaker at 150 rpm for 24 h for all experiments except the kinetic study. After mixing, the mixtures were centrifuged at 5,000 rpm for 5 min, and the supernatants were passed through 0.22 μm filters before being analyzed for ethidium and metal cation concentrations. All experiments were run in duplicate.

We try to use three models like pseudo-second-order, intraparticle diffusion and pseudo-first-order. The r^2 of pseudo-second-order was 0.999 in this study indicated that it was the best-fit model. As for the models to fit the isotherm data, the r^2 of Freundlich was 0.233, and the r^2 of Langmuir was 0.998 in this study which also indicated that it was best-fit model. The well-standard S-type curve of isotherm also implied the Langmuir instead of Freundlich (Fig. 2). Therefore, the data were fitted with the pseudo-second-order
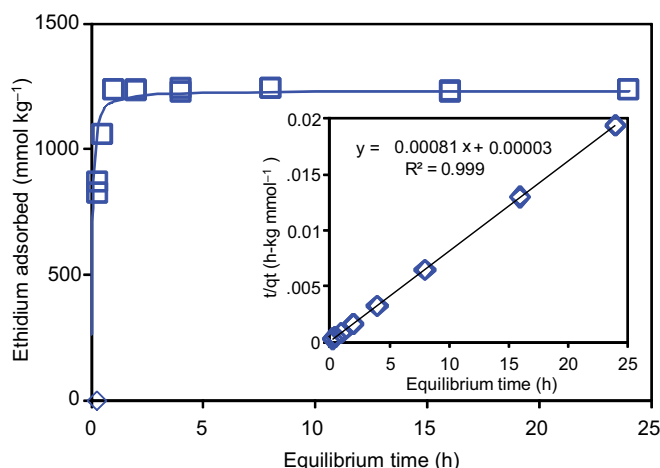
Fig. 1. Kinetics of ethidium adsorption on SAz-1 at pH 7 under an initial concentration of 8 mmol L^{-1}. The curve was a pseudo-second-order rate equation fitted to the data with its linear form illustrated in the inset.
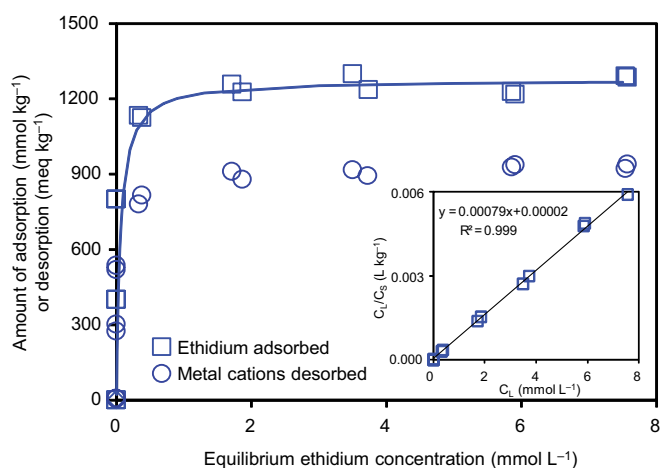
Fig. 2. Adsorption of ethidium bromide on SAz-1 associated with desorption of metal cations at pH 7. The solid curve is the Langmuir fit to the observed data rearranged in a linear form in the insert.

kinetic model and the Langmuir adsorption isotherm model to achieve best-fit scenarios. The integrated rate law of the pseudo-second-order kinetic model is:

$$q_t = \frac{kq_e^2 t}{1 + kq_e t} \tag{1}$$

where k (kg mmol^{-1} h^{-1}) is the rate constant of adsorption, q_e (mmol kg^{-1}) is the amount of ethidium adsorbed at equilibrium, and q_t (mmol kg^{-1}) is the amount of ethidium adsorbed on the adsorbent at time t. The rate-limiting step is chemisorption that includes valence forces through sharing or exchange of electrons between adsorbent and adsorbate and the adsorption capacity is proportional to the number of active sites on the adsorbent, which has been applicable to many adsorption processes [19,20]. Eq. (1) can be re-arranged into a linear form (Eq. 2):

$$\frac{t}{q_t} = \frac{1}{kq_e^2} + \frac{1}{q_e}t \tag{2}$$

where kq_e^2 is the initial rate (mmol kg^{-1} h^{-1}).

The Langmuir adsorption isotherm model can be described as:

$$C_S = \frac{K_L S_m C_L}{1 + K_L C_L} \tag{3}$$

where C_S is the amount of adsorbate adsorbed on adsorbent at equilibrium (mmol kg^{-1}), C_L is the equilibrium solute concentration (mmol L^{-1}), S_m is the apparent adsorption capacity or adsorption maximum (mmol kg^{-1}), and K_L is the Langmuir coefficient (L mmol^{-1}). Eq. (3) can be rearranged to a linear form Eq. (4) and K_L and S_m can be determined by a linear regression.

$$\frac{C_L}{C_s} = \frac{1}{K_L S_m} + \frac{C_L}{S_m} \tag{4}$$

2.3. Methods of analyses

The concentration of ethidium was quantified by a UV-Vis spectrophotometer (SmartSpec 3000, Bio-Rad Corp., USA) at the wavelength of 480 nm [21]. The standards were adjusted to have the same pH as that of the sample supernatants and the calibration was made with five standards between 0.01 and 0.2 mmol L^{-1} with r^2 values no less than 0.998.

The metal cations desorbed from SAz-1 in the solution during the adsorption of ethidium were analyzed by ion chromatography (Dionex 100, Dionex, USA) with an IonPac CS12A column (4 × 250 mm) and a mobile phase made of 1.3 mL of 20 mM methanesulfonic acid in 1 L of water. At a flow rate of 1 mL min^{-1}, the retention times for Na$^+$, K$^+$, Mg^{2+}, and Ca^{2+} were 4.4, 6.2, 10.5, and 13.4 min, respectively.

Powder X-ray diffraction (XRD) patterns of the raw SAz-1 and ethidium-loaded samples were recorded on a Bruker D8 ADVANCE diffractometer with a Sol-X detector and CuKα radiation. X-ray intensities were measured in the range of 2°–20° 2θ at a scan rate of 2°min^{-1} and a step size of 0.01°.

FTIR spectra of the clay samples prepared with the KBr pressing method were acquired on a Thermo Nicolet 6700 spectrometer (Thermo Scientific, USA). The spectra were recorded from 400 to 4,000 cm^{-1} by accumulating 256 scans at a resolution of 4 cm^{-1}.

Thermogravimetric (TG) analyses were performed on a PerkinElmer TGA 4000 instrument at a heating rate of 10°C min^{-1} under N$_2$ condition. The initial sample weight was 5–7 mg.

A helium ion microscope (Orion™ Plus HIM, Carl Zeiss) was used to obtain high-resolution high-contrast secondary electron images for surface features of clay samples without coating. A gas field ion source with helium supplied at a pressure of 2 × 10^{-6} Torr, an accelerating voltage of 25 kV, a bean current of 1.39–1.51 pA, a beam limiting aperture of 10 μm, and a working distance of 6–10 mm were used for the imaging work. In addition, the HIM was

equipped with an electron flood gun to minimize charging effects on specimen surface.

3. Results and discussion

3.1. Adsorption kinetics

The removal of ethidium by SAz-1 reached equilibrium in about 1 h (Fig. 1), which was fast in comparison to 24 h required for the equilibrium adsorption of a variety of organic molecules onto clay minerals [22–25]. The pseudo-second-order kinetic model yielded the best fitting with r^2 equal to 0.999 (Fig. 1). The initial rate kq_e^2 Eq. (2) was 33,333 mmol kg^{-1} h^{-1}, the rate constant k was 0.022 kg mmol^{-1} h^{-1}, and the amount of equilibrium adsorption q_e was 1,235 mmol kg^{-1}, when the kinetic data were fitted to Eq. (2) (Fig. 1). The q_e value agreed well with the adsorption capacity of 1,276 mmol kg^{-1} obtained from the adsorption isotherm experiments in the next section (Fig. 2).

In comparison, the equilibrium time for ethidium bromide removal from aqueous solution was 3.5 h by natural and aluminum-coated pumice [6], 1 h by rectorite [13] and other montmorillonite clays [14], 17 min by graphene oxide [5,26], 15 min by fennel seed spent [27], or a few minutes by nanomaterials [7,8,10] (Table S2). For SAz-1, the adsorption reached to 70% of its maximum capacity within 15 min at the initial concentration of 8 mmol L^{-1} (3,152 mg L^{-1}), which indicated that SAz-1 has an advantage for fast removal of a high quantity of ethidium bromide from aqueous solution.

3.2. Adsorption isotherm

The adsorption isotherm data were best fitted with the Langmuir adsorption model with an r^2 value of 0.998 (Fig. 2). The adsorption capacity S_m was 1,276 mmol kg^{-1} (Fig. 2), much higher than 149 mmol kg^{-1} (58.82 mg g^{-1}) and 195 mmol kg^{-1} (76.92 mg g^{-1}) reported for adsorption of ethidium bromide on natural pumice and aluminum-coated pumice at solution pH 8 [6], and the value was also several times larger than the adsorption of 406 mmol kg^{-1} (160 mg g^{-1}) on rectorite [13] and 334 mmol kg^{-1} (131.76 mg g^{-1}) on fennel seed spent [27] (Table S1). The adsorption capacity of 1,276 mmol kg^{-1} approximates the CEC value of SAz-1 (1,230 meq kg^{-1}), implying adsorption dominated by cation exchange.

3.3. Desorption of exchangeable cations

There were many previous studies displayed the desorption analysis would resolve the mechanism [8–10, 12–14,24,25]. Thus, to confirm cation exchange mechanism, desorption of metal cations was also quantified in this study. In association with the adsorption of ethidium, the metal cations desorbed from SAz-1 were mainly Ca^{2+} and Mg^{2+} and the total amount of desorbed cations in equivalent charge (in meq kg^{-1}) had a positive linear correlation (r^2 = 0.99) with the amount of ethidium adsorbed (Fig. 3). Such a linear relationship further implied that cation exchange was the dominant mechanism for ethidium adsorption on SAz-1. However, the slope of such a linear correlation was 0.72 (Fig. 3), indicating that in addition to
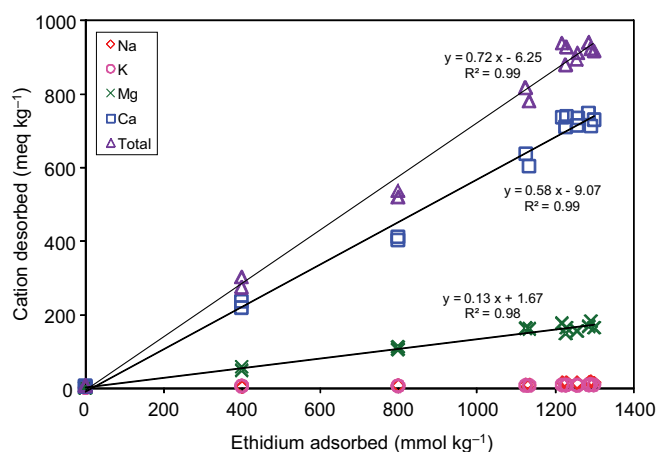
Fig. 3. Amounts of desorbed metal cations from SAz-1 as a function of the amount of ethidium adsorption.

cation exchange other mechanism may also play a role, or the adsorbed ethidium could occur in forms other than monovalent ethidium monomers.

3.4. Effects of solution pH and ionic strength

The point of zero charge (PZC) of an adsorbent may play an important role in the variation of its adsorption capacity with solution pH when electrostatic interaction is the key mechanism for adsorption [28]. The PZC of SAz-1 was pH 7.7 [29], which indicated that the pH-dependent surface of SAz-1 would be positively charged and the adsorption could be reduced at solution pH < 7.7 when the adsorbate was in form of cationic molecules. However, most of the surface charges of SAz-1 are permanent surface charges due to isometric substitution in the tetrahedral or octahedral sheets. As such, the adsorption of ethidium on SAz-1 was not reduced at pH 5–7 and a moderate reduction of the adsorption by about 17% occurred at pH 2–4 (Fig. 4a), which indicated that the influence by solution pH could be largely due to competitive adsorption from H$^+$ ions (protonation) on the pH-dependent sorption sites, consistent with cation exchange as the dominant mechanism for ethidium adsorption on SAz-1. Similar effects were also observed for amitriptyline and ciprofloxacin adsorption on Ca-montmorillonite [30,31].

The addition of a second cation can lower the uptake of cationic adsorbate by adsorbent when the adsorption is dominated by cation exchange. However, such a competition effect was not observed by the minute and unsystematic variation in the amount of ethidium adsorption on SAz-1 as the ionic strength made with dissolved NaCl or CaCl$_2$ increased (Fig. 4b). The result indicated a high affinity of ethidium for SAz-1 in aqueous solution at neutral pH in the presence of Na$^+$ and Ca^{2+} cations, suggesting that the organic cations have a higher affinity for the negatively charged montmorillonite surfaces in comparison to inorganic cations. This might be attributed to ion-dipole interactions of the amine groups of ethidium with the SAz-1 surface as implied by the FTIR result described.
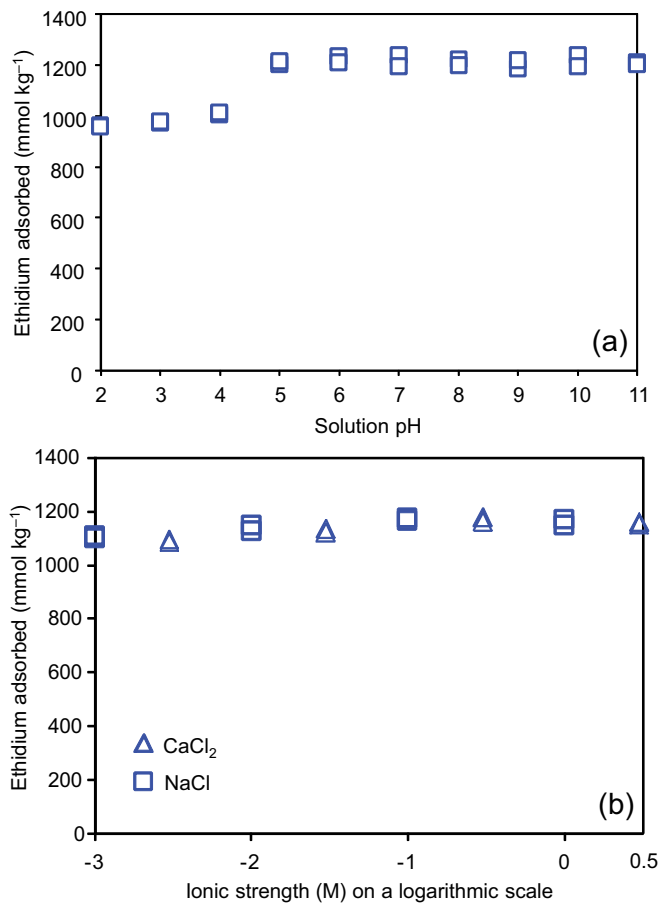
Fig. 4. Ethidium uptake on SAz-1 as affected by equilibrium solution pH (a) and ionic strength (b) at an initial concentration of 8 mmol L^{-1}.

3.5. Effect of temperature on ethidium adsorption

At neutral pH and an initial concentration of 8 mmol L^{-1}, the adsorption capacity of ethidium on SAz-1 decreased slightly with increasing temperature (Fig. 5), suggesting weakly exothermic for the adsorption. The thermodynamic parameters of the adsorption can be deduced from the values of partitioning coefficient (K_d) at 303, 318, and 333 K using the following equation:

$$\ln K_d = -\frac{\Delta H}{RT} + \frac{\Delta S}{R} \tag{5}$$

where T is the temperature in K, R is the gas constant (8.314 J mol^{-1} K^{-1}), and ΔH and ΔS are the changes of enthalpy and entropy through adsorption. The Gibbs free energy of adsorption, ΔG is related to these thermodynamic parameters by the equation of:

$$\Delta G = \Delta H - T\Delta S \tag{6}$$

The negative ΔG values in this study suggested a spontaneous adsorption process (Table 1), which could indicate a high affinity between SAz-1 and ethidium in the adsorption [8,32,33]. The adsorption was exothermic with a
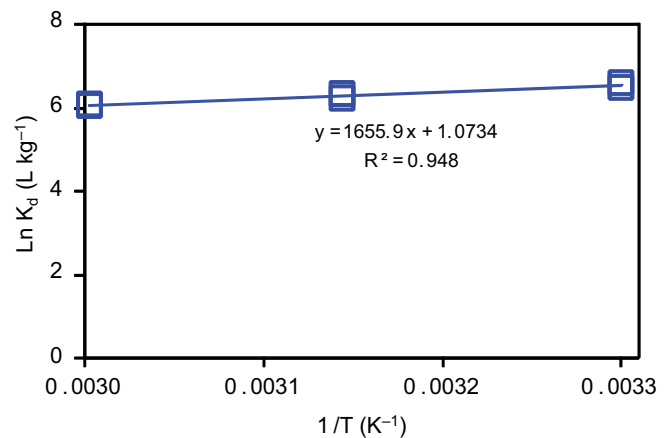
Fig. 5. Ethidium adsorption on SAz-1 with an initial concentration of 8 mmol L^{-1} at solution pH 7 at 303, 318, and 333 K.

negative ΔH value. In contrast, the adsorption of ethidium bromide on carbon nanotubes was endothermic [8]. In addition, the change of entropy, ΔS was minimal and the order–disorder state was virtually unchanged through the uptake of ethidium by SAz-1 in aqueous solution.

3.6. X-ray diffraction analysis

The d$_{001}$ value increased from 15.5 Å for raw SAz-1 to 16.5 and 18.3 Å as the loading of ethidium on SAz-1 increased (Fig. 6a). No further increase of the basal spacing was observed after the adsorption corresponding to 1.04 CEC of SAz-1 was reached at an initial concentration of 8 mmol L^{-1} (Fig. 2). At the same initial concentration of 8 mmol L^{-1}, the d_{001} values of the ethidium-loaded samples remained more or less the same at solution pH 2 to 11 (Fig. 6b).

Collapsing of the basal spacing to 10 Å upon dehydration at 300°C–350°C with a further reduction to 9.6 Å at 500°C–600°C due to dehydroxylation are diagnostic of natural Ca-montmorillonite [34]. In this study, the d$_{001}$ values of SAz-1 with different ethidium loadings decreased to 13–17 Å upon heating at 500°C and to 10.5–12.1 Å at 600°C (Fig. 7), much greater than the basal spacing of 9.6 Å for raw SAz-1 heated at 500°C and 600°C. The clay layers were probably shielded by partially decomposed ethidium with little or no dehydroxylation at 500°C, and dehydroxylation of the clay layers and further decomposition of intercalated ethidium into carbonaceous residues occurred at 600°C.

3.7. Thermogravimetric analyses

At temperatures lower than 200°C, the mass losses of raw SAz-1 and SAz-1 loaded with different amounts of ethidium were largely due to dehydration of interlayer water (Fig. 8a). The dehydration mass loss decreased with increasing adsorption of ethidium in substitution for interlayer cation-water complexes and was 5%–6% when the amount of ethidium adsorption was equivalent to about 1 CEC of the clay. The temperature for the decomposition of raw ethidium bromide spanned largely in the range of 250°C–450°C and peaked at 353°C (Fig. 8b) in comparison to the onset melting and decomposition temperature

Table 1
Thermodynamic parameters of ethidium bromide adsorption on SAz-1 at solution pH 7 under different temperatures

ln(K_d) (L kg^{-1})			ΔG (kJ mol^{-1})			ΔH (kJ mol^{-1})	ΔS (kJ mol^{-1} K^{-1})
303 K	318 K	333 K	303 K	318 K	333 K		
6.55	6.27	6.05	−16.47	−16.61	−16.74	−13.77	0.01
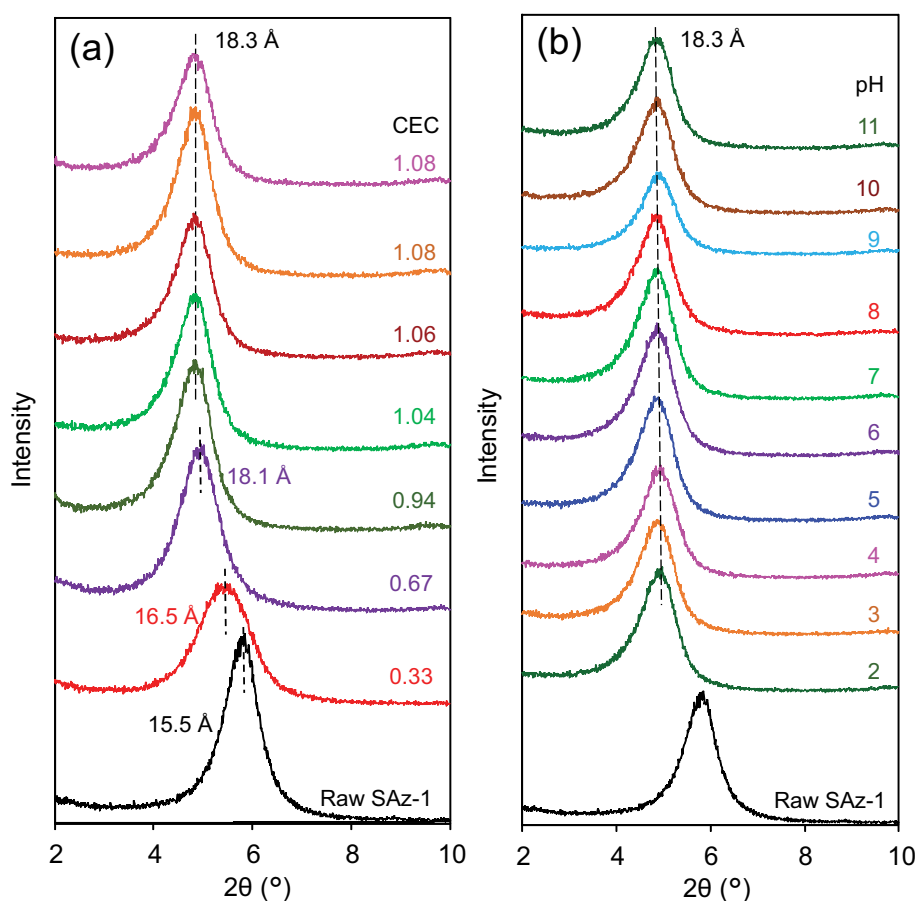
Fig. 6. XRD patterns of raw SAz-1 and SAz-1 with different amounts of ethidium adsorption at pH 7 (a) and SAz-1 with an ethidium loading equivalent to 1.04 CEC of the clay at solution pH 2–11 (b).

of 262°C or 255°C–266°C [35,36]. For SAz-1 with low and high loading levels of ethidium, there was a broad mass-loss peak centered at ca. 384°C and 362°C, respectively (Fig. 8b), slightly higher than 353°C, implying slightly enhanced thermal stability for adsorbed ethidium. Thermal stability of organic molecules could be enhanced through shielding when adsorptively intercalated into the interlayer of swelling clay minerals [13,30], and there appeared to be slightly different shielding effects due to different adsorbed states of ethidium on SAz-1 at low and high loading levels with adsorbed ethidium molecules associated with different amounts of hydrated metal cations. Two adsorbed states of ethidium including adsorption on the external surface and intercalation in the smectitic interlayer of rectorite were implied by the simultaneous occurrence of two mass-loss peaks at high loading levels [13]. The mass losses at 500°C–600°C (Fig. 8a) could be largely attributed

to dehydroxylation of SAz-1 and progressive decomposition of ethidium intercalated in the interlayer of SAz-1, as also evidenced from the decreases of the basal spacings illustrated in the previous section.

3.8. HIM imaging

Raw SAz-1 consisted of massive stacks of largely coalescing flakes with ill-defined boundaries, low surface reliefs, and local curvy edges (Fig. S2a, c, e). In contrast, ethidium-adsorbed SAz-1 contained fragmented blocks composed of stacks of flakes largely disconnected by stepped edges or gaps (Fig. S2b, d, f), probably related to layer expansion in SAz-1 due to ethidium intercalation. Compared to electron beams, the focused helium ion source is capable of producing secondary electrons with great efficiency sensitive to specimen composition. At nearly identical
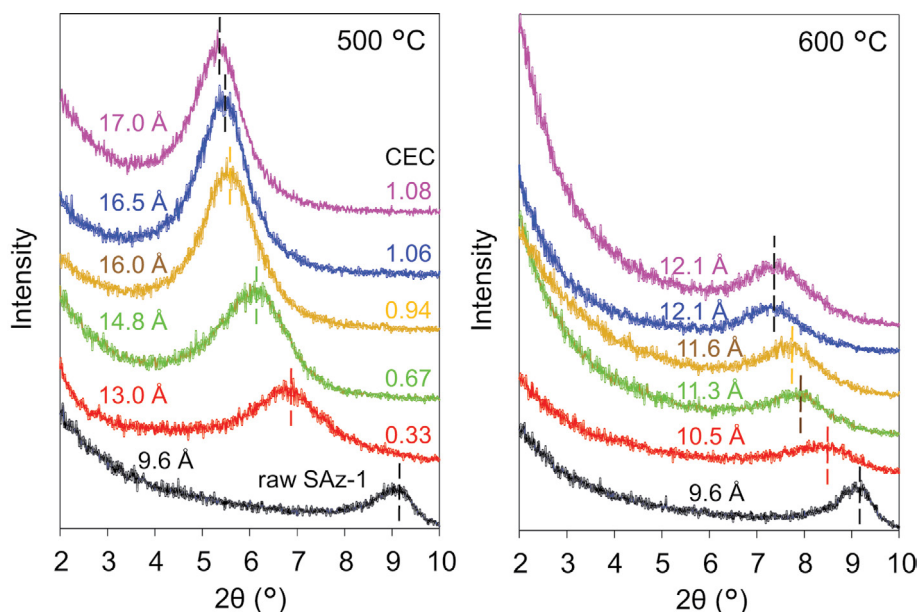
Fig. 7. XRD patterns of raw SAz-1 and SAz-1 with different amounts of ethidium adsorption after being heated to 500°C and 600°C.

instrumental settings, the secondary electron images of ethidium-adsorbed SAz-1 exhibited much enhanced brightness and contrast relative to those for raw SAz-1 (Fig. S2). As ethidium molecules have a low average atomic number, the enhanced signal implied that the adsorption of ethidium onto SAz-1 could be partially associated with bromine counterions. A similar effect was also suggested for the case of ethidium bromide adsorption onto rectorite [13].

3.9. FTIR analyses

The bands at 463; 517; 623; 847; 916; 1,030; 1,109; 1,636; 3,247; 3,426 and 3,628 cm^{-1} for raw SAz-1 (Fig. 9) were attributed to Si–O–Si deformation, Al–O–Si deformation, coupled Al–O and Si–O out-of-plane bending, AlMgOH deformation, AlAlOH deformation, Si–O in-plane stretching, Si–O stretching longitudinal mode, OH deformation of water, OH stretching of water, and OH stretching of structural hydroxyl groups, respectively [37]. The 3,196 and 3,278 cm^{-1} bands of raw ethidium bromide (Fig. 9a) were related to the 3,192 and 3,302 cm^{-1} bands (Table 2) which were previously assigned to NH$_2$ symmetric and asymmetric stretching vibrations for 4-aminoantipyrine [38]. These two bands shifted to 3,207 and 3,378 cm^{-1} after ethidium adsorption on SAz-1 (Table 2), implying strong interactions between the amine groups of the ethidium molecules and SAz-1 [32]. In addition, active ν(C=C) stretching was evidenced by the band shift from 1,478 to 1,500 cm^{-1} (Fig. 9b), suggesting an adjustment of the aromatic rings of ethidium [38] after adsorption. The result supported that the positive charge of amine groups of ethidium actively participated in the adsorptive interaction with the SAz-1 surface.

3.10. Mechanism of ethidium bromide removal

The intercalation of ethidium in the interlayer of SAz-1 was supported by the expansion of d_{001} to 18.3 Å for SAz-1
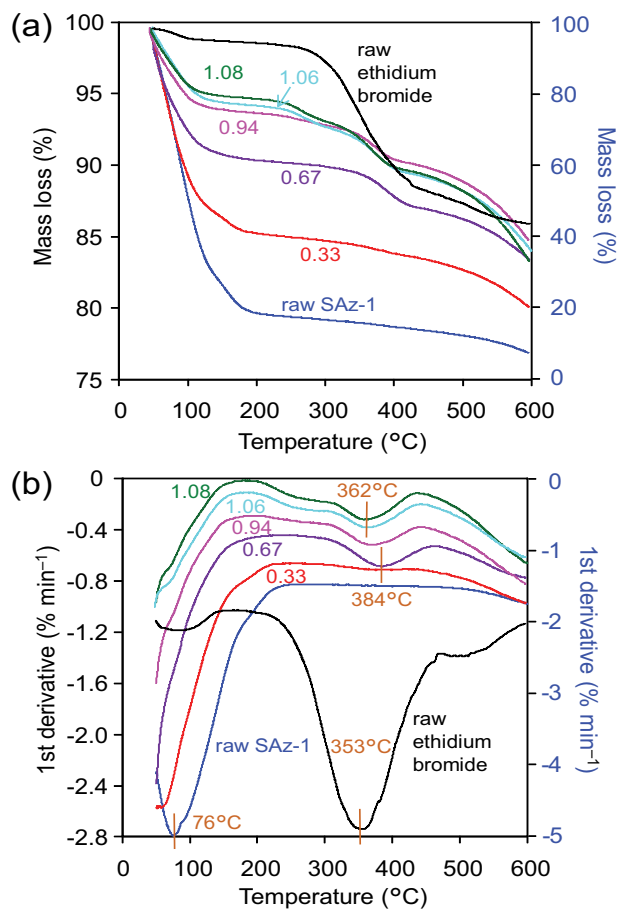
Fig. 8. TG analyses of raw ethidium bromide and SAz-1 with different amounts of ethidium adsorption expressed as equivalent CEC values (a), and their first derivatives (b). The vertical scale on the right is for raw ethidium bromide and raw SAz-1 and the scale on the left for ethidium-adsorbed SAz-1 samples.

Fig. 9. FTIR spectra of raw SAz-1 and ethidium bromide and SAz-1 with different amounts of ethidium adsorption corresponding to the CEC value of SAz-1 in the wavenumber ranges of 400–4,000 cm^{-1} (a) and 400–1,800 cm^{-1} (b).

at high loading levels (Fig. 6) and the elevated decomposition temperature of the intercalated molecules (Figs. 7 and 8). The clay samples with low and high loading levels of ethidium exhibited a mass-loss plateau peaked at 384°C and 362°C, respectively (Fig. 8b), and the decomposition plateau gradually shifted its peak towards 362°C as the adsorption increased. The occurrence of two mass-loss peaks upon heating could be attributed to the decomposition of surface adsorbed and intercalated ethidium bromide molecules, with increased surface adsorption at high adsorption levels, similar to the adsorption of ethidium bromide on rectorite in which two mass-loss peaks at 360°C and 420°C were detected for rectorite with an uptake of 400 mmol kg^{-1} which was about the CEC value of the clay [13].

Cation exchange was the dominant adsorption mechanism as suggested by the positive linear relationship between the amounts of desorbed cations and adsorbed ethidium and partially supported by the intercalation of ethidium in the interlayer of SAz-1. However, the desorption of metal cations and the adsorption of ethidium kept a ratio of 0.72 in equivalent charge, which could not be accounted by just cation exchange alone. However, the less-than-unity ratio may indicate different forms of ethidium on the surface or in the interlayer of SAz-1.

The total surface area of SAz-1 was reported to be 736 m^2 g^{-1} that included the external surface area and the interlayer area available for adsorption [18]. When a monolayer adsorption was assumed, the coverage was 0.54, 1.09, 1.53, 1.69, 1.74, and 1.75 μmol m^{-2} or 0.24, 0.47, 0.67, 0.73, 0.75, and 0.76 molecule per 100 Å^2, and the occupied area per adsorbed ethidium molecule was 306, 153, 108, 98, 96, and 95 Å^2 at loading levels equivalent to 0.33, 0.65, 0.92, 1.01, 1.04, and 1.05 CEC of SAz-1. The molecular size of ethidium is 10 × 11 × 5 Å with a flat-lying area of 110 Å^2. Thus, the surface area of SAz-1 became inadequate for a monolayer coverage of flat-lying ethidium molecules as the loading approached ca. 1 CEC. Consequently, tilting or stacking of

Table 2
Band positions (cm^{-1}) and assignments for FTIR spectra of ethidium bromide

Raw EtBr[a]	Adsorbed EtBr	EtBr band assignment [32]	
3278	3378	3302	ν(N–H)
3196	3207	3192	ν_{as}(C–H); ν(C–H); ν(NH$_3^+$)
1629	1629	1629	δ(N–H)
1568	1578	1578	δ(NH$_3^+$)$_{def}$; ν(C=C) (in ring); ν(C=N); δ(C–H) deformation; ring breathing bands
1496	1498	1499	ν(C=N)
1478	1500	1489	ν(C=C) (in-ring)
1404	1406	1408	ν(C–H); δ(C–H) deformation
1350	1350	1352	ν(C–C) + ν_{as}(C–N); C–H rock, alkanes
1317	1317	1319	ν_s(C–N)
1261	1265	1262	ρ(NH$_3^+$)
1203	1203	1207	δ(C–H) in plane bending
837	837	837	C–H out of plane bending
771	771	773	N–H wag; C–H out of plane bending; skeletal vibrations
704	704	706	CNC deformation

[a]EtBr = ethidium bromide.

adsorbed ethidium molecules was required for adsorption at high loading levels.

As evidenced from the FTIR results, the adsorptive interaction was dominated by the contact between the amine groups of ethidium and the basal oxygen of SAz-1. Such an interaction contact might be facilitated with adsorbed ethidium monomers having long axis tilted >37° away from the flat-lying posture could fit into the interlayer space at high loadings and the contact area would be reduced by at least 20%. Thus, the adsorption capacity would not be limited by the total surface area of SAz-1 with such an adsorption configuration.

The stacking of adsorbed ethidium molecules could occur in the form of a bilayer conformation or flat-lying dimeric aggregates with aromatic rings parallel to the basal plane of SAz-1. The stacking height would be about twice of the height of an ethidium molecule and the surface coverage would be halved at high loading levels. Interlayer intercalation of ethidium with a bilayer conformation was proposed for adsorption on Ca-montmorillonite at the loading level of 1.5 mmol g^{-1} with molecular simulation [14]. However, simply an incline or a bilayer conformation of ethidium molecules in the interlayer could not adequately account for the less-than-unity proportion of cation desorption to ethidium adsorption in equivalent charge.

Dye molecules could form monomer, dimer, or other types of aggregation depending on dye concentrations in aqueous solution and notable effects on aggregation state of dye molecules by clay mineral's surface area, surface charge density, swelling capacity, loading level, and intercalation configuration could occur when dye molecules were adsorbed on clay minerals [39–42]. The reported dimerization constant for dimeric ethidium (Et_2) was 133 L mol^{-1} [43]

or 96 ± 10 M^{-1} [44] at 303 K. When the ethidium molecules were dominated by monomers and dimers equilibrated with the dimerization constant of 133 L mol^{-1} at the initial concentration of 2, 4, 6, 8, 10, 12, and 14 mmol L^{-1}, the equilibrium dimer concentration would be 0.28, 0.78, 1.39, 2.04, 2.73, 3.45, and 4.19 mM with the dimer to monomer concentration ratio of 0.19, 0.32, 0.43, 0.52, 0.60, 0.68, and 0.75, respectively. Thus, ethidium dimers could have formed a significant proportion in aqueous solution at any of the initial concentrations prior to adsorption. In addition, various elevated degrees of dimerization and changes of fluorescence properties of dye molecules could occur upon their adsorption onto clay minerals. For example, apparently induced dimerization and metachromasy of dye molecules had been demonstrated with spectroscopic measurements for acridine orange and methylene blue adsorbed onto montmorillonite in aqueous suspension [41,45,46], and the state of dye aggregation could be adjusted by reducing layer charge in smectitic clays [42,47]. Ethidium dimer could occur in the form of a stacked complex consisting of two ethidium molecules in a parallel orientation [48]. Dimerization of ethidium molecules associated with bromide and fluorescence quenching effects were reported for adsorption on rectorite at high loading levels [13]. Although no direct measurements of absorption and fluorescence spectra were made in this study, a high proportion of ethidium dimers upon adsorption on SAz-1 at any of the initial concentrations was conceivable. The adsorbed ethidium could include a combination of monovalent monomers, Et^+ and dimers associated with Br^-, $(Et_2Br)^+$ and such an assemblage could yield a way to arrive at a less-than-unity ratio of desorption and adsorption in equivalent charge.
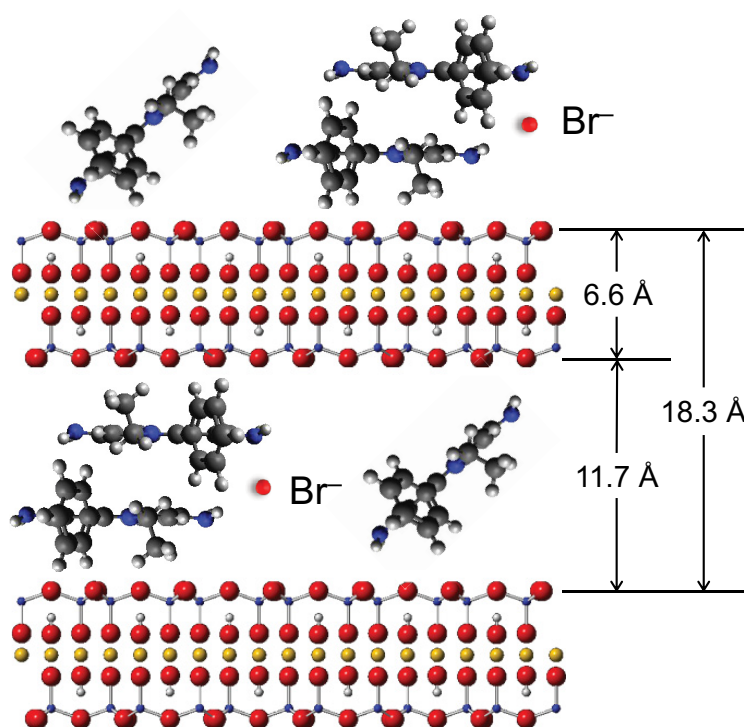
Fig. 10. Schematic illustration for adsorption of ethidium dimers associated with Br^- on Ca-montmorillonite.

An adsorbed admixture of Et^+ monomers and $(Et_2Br)^+$ dimers with a molar ratio of ca. 1.6 (=44/28) could contribute to 44% and 56% of the total amount of ethidium adsorption on SAz-1, and exchange with the desorbed metal cations taking up 72% of the equivalent charge of the CEC of SAz-1 at the full adsorption level. Under these conditions, the occupied area per ethidium monomer or dimer on average would be ca. 130 Å^2 which is larger than 110 Å^2, the lateral area of a flat-lying ethidium monomer or dimer. Thus, external surface adsorption and interlayer intercalation of flat-lying ethidium molecules partially involving dimeric aggregation and bromide association without tilting were feasible for highly efficient removal of ethidium bromide by Ca-montmorillonite from aqueous solution (Fig. 10). Under these conditions, the conformation of adsorbed ethidium monomers was not well constrained by steric effects but molecular tilting might facilitate comparatively low surface coverage at high loading levels and active interaction of the amine groups of ethidium with the basal surface of the clay.

Previous results showed that the ethidium saturated montmorillonite could be heat regenerated [14]. The results in this study suggest that the heat regeneration could be due to combined effect of thermal destruction of ethidium and lack of sorbed/intercalated cations to balance the net negative charges of montmorillonite. Thus, theoretically speaking, the heat regenerated montmorillonite not only can be used to remove ethidium bromide, but also other organic and inorganic cations, another advantage of using montmorillonite for the removal of ethidium bromide from solution.

4. Conclusion

The removal of ethidium bromide by Ca-montmorillonite SAz-1 was highly effective with equilibrium reached within 1 h and the adsorption obeyed the Langmuir isotherm model with an adsorption capacity of 1,276 mmol kg^{-1} (503 mg g^{-1}), approximately equivalent to the CEC value of SAz-1. The desorption of metal cations from SAz-1 and the adsorption of ethidium were linearly related with a slope of 0.72 in equivalent charge. Thus, the adsorption was dominated by a cation exchange interaction. Such a less-than-unity ratio of charge exchange and the expansion of the basal spacing of SAz-1 after adsorption further implied that interlayer intercalation of monovalent monomers and flat-lying dimers of ethidium partially associated with counterion Br$^-$ was involved in the effective uptake by SAz-1. For fast, high-performance removal of ethidium bromide from aqueous solution, low-cost Ca-montmorillonite is a notable adsorbent and it can be highly effective in the instance of spill incidents in particular.

Acknowledgements

References

[1] V.L. Singer, T.E. Lawlor, S. Yue, Comparison of SYBR Green I nucleic acid gel stain mutagenicity and ethidium bromide mutagenicity in the Salmonella/mammalian microsome reverse mutation assay (Ames test), Mutat. Res., 439 (1999) 37–47.

[2] S. Thititananukiji, R. Vejaratpimol, T. Pewnim, A.W. Fast, Ethidium bromide nuclear staining and fluorescence microscopy: an alternative method for triploidy detection in fish, J. World Aquacult Soc., 27 (2010) 213–217.

[3] M. Waring, Ethidium and Propidium, J.W. Corcoran, F.E. Hahn, J.F. Snell, K.L. Arora, Eds., Mechanism of Action of Antimicrobial and Antitumor Agents. Antibiotics 3, Springer, Berlin, 1975, pp. 141–165. Available at: https://doi.org/10.1007/978-3-642-46304-4_10

[4] S. Amirijavid, M. Mohammadi, Toxicity of the ethidium bromide on germination of wheat, alfalfa and tomato, Int. J. Agric. Soil Sci., 2 (2014) 69–74.

[5] M. Rajabi, O. Moradi, K. Zare, Kinetics adsorption study of the ethidium bromide by graphene oxide as adsorbent from aqueous matrices, Int. Nano Lett., 7 (2017) 35–41.

[6] B. Heibati, K. Yetilmezsoy, M.A. Zazouli, S. Rodriguez-Couto, I. Tyagi, S. Agarwal, V.K. Gupta, Adsorption of ethidium bromide (EtBr) from aqueous solutions by natural pumice and aluminium-coated pumice, J. Mol. Liq., 213 (2016) 41–47.

[7] A. Fakhri, Assessment of Ethidium bromide and Ethidium monoazide bromide removal from aqueous matrices by adsorption on cupric oxide nanoparticles, Ecotoxicol. Environ. Saf., 104 (2014) 386–392.

[8] O. Moradi, A. Fakhri, S. Adami, S. Adami, Isotherm, thermodynamic, kinetics, and adsorption mechanism studies of Ethidium bromide by single-walled carbon nanotube and carboxylate group functionalized single-walled carbon nanotube, J. Colloid Interface Sci., 395 (2013) 224–229.

[9] R.G. Harris, J.D. Wells, B.B. Johnson, Selective adsorption of dyes and other organic molecules to kaolinite and oxide surfaces, Colloids Surf., A, 180 (2001) 131–140.

[10] F. Najafi, M. Norouzi, K. Zare, A. Fakhri, Removal of ethidium bromide by carbon nanotube in aqueous solution: isotherms, equilibrium mechanism studies, and its comparison with nanoscale of zero valent iron as adsorbent, J. Nanostruct. Chem., 3 (2013) 60, doi: 10.1186/2193-8865-3-60.

[11] G.D. Yuan, B.K.G. Theng, G.J. Churchman, W.P. Gates, Clays and Clay Minerals for Pollution Control, F. Bergaya, G. Lagaly, Eds., Handbook of Clay Science, 2nd ed., Elsevier, Amsterdam, 2013, pp. 587–644. Available at: https://doi.org/10.1016/S1572-4352(05)01020-2

[12] B. Sarkar, R. Rusmin, U.C. Ugochukwu, R. Mukhopadhyay, K.M. Manjaiah, Modified Clay Minerals for Environmental Applications, M. Mercurio, B. Sarkar, A. Langella, Eds., Modified Clay and Zeolite Nanocomposite Materials, Elsevier, Amsterdam, 2019, pp. 113–127. Available at: https://doi.org/10.1016/B978-0-12-814617-0.00003-7

[13] Z. Li, P.-H. Chang, W.-T. Jiang, Y.-J. Liu, Enhanced removal of ethidium bromide (EtBr) from aqueous solution using rectorite, J. Hazard. Mater., 384 (2020) 121254, doi: 10.1016/j.jhazmat.2019.121254.

[14] L. Wang, Z. Li, X. Zhang, G. Lv, X. Wang, High capacity ethidium bromide removal by montmorillonites, Korean J. Chem. Eng., 37 (2020) 2202–2208.

[15] Z. Zimmermann, H.W. Zimmermann, pKa-Werte von Ethidiumbromid und 7-Amino-9-phenyl-10-äthyl-phenanthridinium-bromid, Zeitschrift für Naturforschung C, 31 (1976) 656–660.

[16] S.J. Chipera, D.L. Bish, Baseline studies of the Clay Minerals Society source clays: powder X-ray diffraction analyses, Clays Clay Miner., 49 (2001) 398–409.

[17] A. Umran Dogan, M. Dogan, M. Onal, Y. Sarikaya, A. Aburub, D.E. Wurster, Baseline studies of the Clay Minerals Society source clays: specific surface area by the Brunauer Emmett Teller (BET) method, Clays Clay Miner., 54 (2006) 62–66.

[18] G. Villemure, Effect of negative surface-charge densities of smectite clays on the adsorption isotherms of racemic and enantiomeric tris(2,2'-bipyridyl)ruthenium(II) chloride, Clays Clay Miner., 38 (1990) 622–630.

[19] Y.S. Ho, G. McKay, Pseudo-second-order model for sorption processes, Process Biochem., 34 (1999) 451–465.

[20] Y. Park, G.A. Ayoko, E. Horváth, R. Kurdi, J. Kristof, R.L. Frost, Structural characterisation and environmental application of organoclays for the removal of phenolic compounds, J. Colloid Interface Sci., 393 (2013) 319–334.

[21] J. Carbajo, C. Adán, A. Rey, A. Martínez-Arias, A. Bahamonde, Optimization of H_2O_2 use during the photocatalytic degradation of ethidium bromide with TiO_2 and iron-doped TiO_2 catalysts, Appl. Catal., B, 102 (2011) 85–93.

[22] M. Doğan, M. Alkan, A. Türkyilmaz, Y. Özdemir, Kinetics and mechanism of removal of methylene blue by adsorption onto perlite, J. Hazard Mater., 109 (2004) 141–148.

[23] R.A. Figueroa, A. Leonard, A.A. MacKay, Modeling tetracycline antibiotic sorption to clays, Environ. Sci. Technol., 38 (2004) 476–483.

[24] P.-H. Chang, Z. Li, T.-L. Yu, S. Munkhbayer, T.-H. Kuo, Y.-C. Hung, J.-S. Jean, K.-H. Lin, Sorptive removal of tetracycline from water by palygorskite, J. Hazard. Mater., 165 (2009) 148–155.

[25] Z. Li, P.-H. Chang, W.-T. Jiang, J.-S. Jean, H. Hong, L. Liao, Removal of diphenhydramine from water by swelling clay minerals, J. Colloid Interface Sci., 360 (2011) 227–232.

[26] M. Rajabi, O. Moradi, M. Sillanpää, K. Zare, A.M. Asiri, S. Agarwal, V.K. Gupta, Removal of toxic chemical ethidium monoazide bromide using graphene oxide: thermodynamic and kinetics study, J. Mol. Liq., 29 (2019) 111484, , doi: 10.1016/j. molliq.2019.111484.

[27] R. Sulthana, S.N. Taqui, F. Zameer, U.T. Syed, A.A. Syed, Adsorption of ethidium bromide from aqueous solution onto nutraceutical industrial fennel seed spent: kinetics and thermodynamics modeling studies, Int. J. Phytorem., 20 (2018) 1075–1086.

[28] D. Vasudevan, G.L. Bruland, B.S. Torrance, V.G. Upchurch, A.A. MacKay, pH-dependent ciprofloxacin sorption to soils: interaction mechanisms and soil factors influencing sorption, Geoderma, 151 (2009) 68–76.

[29] M. Stadler, P.W. Schindler, Modeling of H^+ and Cu^{2+} adsorption on calcium-montmorillonite, Clays Clay Miner., 41 (1993) 288–296.

[30] P.-H. Chang, W.-T. Jiang, Z. Li, C.-Y. Kuo, J.-S. Jean, W.-R. Chen, G. Lv, Mechanism of amitriptyline adsorption on Ca-montmorillonite (SAz-2), J. Hazard. Mater., 277 (2014) 44–52.

[31] C.-J. Wang, Z. Li, W.-T. Jiang, J.-S. Jean, C.-C. Liu, Cation exchange interaction between antibiotic ciprofloxacin and montmorillonite, J. Hazard. Mater., 183 (2010) 309–314.

[32] H.H. Eldaroti, S.A. Gadir, M.S. Refat, A.M. Adam, Preparation, spectroscopic and thermal characterization of new charge-transfer complexes of ethidium bromide with π-acceptors. In vitro biological activity studies, Spectrochim. Acta, Part A, 109 (2013) 259–271.

[33] B. Sarkar, M. Megharaj, Y. Xi, R. Naidu, Surface charge characteristics of organo-palygorskites and adsorption of p-nitrophenol in flow-through reactor system, Chem. Eng. J., 185–186 (2012) 35–43.

[34] G.W. Brindley, G. Brown, Crystal Structures of Clay Minerals and their X-ray Identification, Mineralogical Society, London, 1980.

[35] P. Quillardet, M. Hofnung, O. Bensaude, Ethidium bromide and safety—readers suggest alternative solutions, Trends Genetics, 4 (1988) 89–90.

[36] F.J. Green, Sigma-Aldrich Handbook of Stains, Dyes, and Indicators, Aldrich Chemical Company, Milwaukee, Wisconsin, 1990.

[37] J. Madejová, P. Komadel, Baseline studies of the Clay Minerals Society source clays: infrared methods, Clays Clay Miner., 49 (2001) 410–432.

[38] J. Swaminathan, M. Ramalingam, V. Sethuraman, G.N. Sundaraganesan, S. Sebastian, Vibrational spectroscopic studies and DFT calculations of 4-aminoantipyrine, Spectrochim. Acta, Part A, 73 (2009) 593–600.

[39] D. Garfinkel-Shweky, S. Yariv, Metachromasy in clay-dye systems: the adsorption of acridine orange by Na-saponite, Clay Miner., 32 (1997) 653–663.

[40] D. Garfinkel-Shweky, S. Yariv, The determination of surface basicity of the oxygen planes of expanding clay minerals by acridine orange, J. Colloid Interface Sci., 188 (1997) 168–175.

[41] J. Bujdák, N. Iyi, Visible spectroscopy of cationic dyes in dispersions with reduced-charge montmorillonites, Clays Clay Miner., 50 (2002) 446–454.

[42] J. Bujdák, Effect of the layer charge of clay minerals on optical properties of organic dyes. A review, Appl. Clay Sci., 34 (2006) 58–73.

[43] A.N. Veselkov, L.N. Dymant, S.F. Baranovskiy, The study of self-association of ethidium bromide in an aqueous solution by H-NMR spectroscopy, Khim Fizika, 13 (1994) 72–80.

[44] M. Guenza, C. Cuniberti, The ethidium bromide dimer. Absorption and fluorescence properties in aqueous solutions, Spectrochim. Acta, Part A, 44 (1988) 1359–1364.

[45] R. Cohen, S. Yariv, Metachromasy in clay minerals. Sorption of acridine orange by montmorillonite, J. Chem. Soc., Faraday Trans. 1 F, 80 (1984) 1705–1715.

[46] J. Cenens, R.A. Schoonheydt, Visible spectroscopy of methylene blue on hectorite, laponite B, and barasym in aqueous suspension, Clays Clay Miner., 36 (1988) 214–224.

[47] J. Bujdák, M. Janek, J. Madejova, P. Komadel, Methylene blue interactions with reduced-charge smectites, Clays Clay Miner., 49 (2001) 244–254.

[48] G. Thomas, B. Roques, Proton magnetic resonance studies of ethidium bromide and its sodium borohydride reduced derivative, FEBS Lett., 26 (1972) 169–175.

Supplementary information
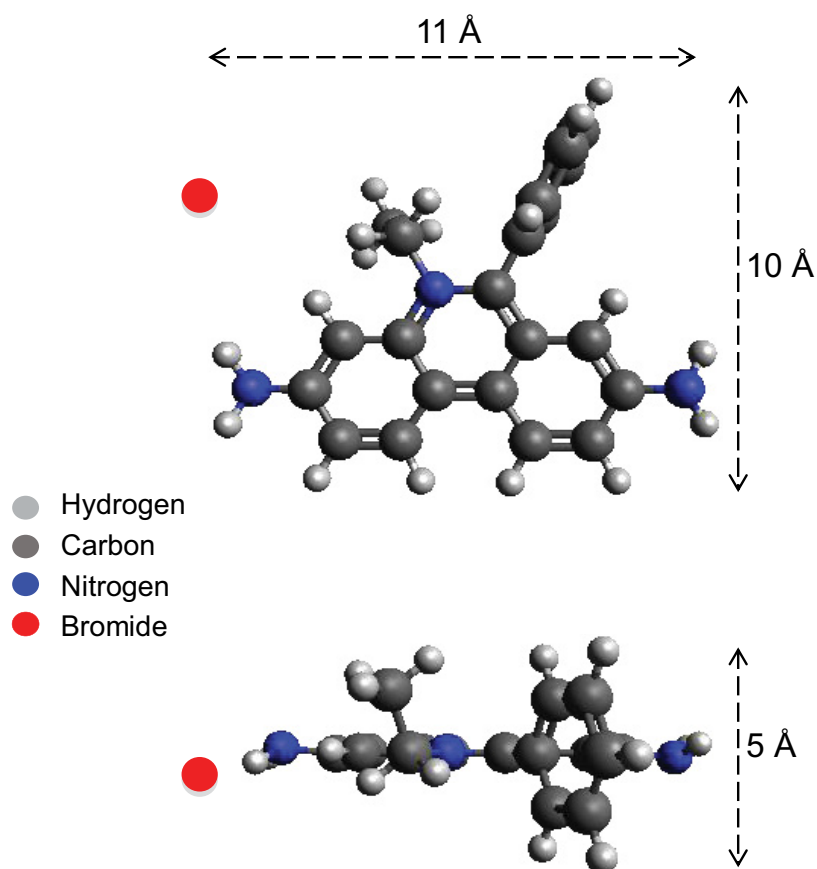
Fig. S1. Molecular structure of ethidium bromide.

Table S1
Properties of adsorbents for removal of ethidium bromide

Adsorbent	CEC	N_2 SSA	Adsorption capacity	Isotherm model
Graphene oxide [5]	Unlisted	133 $m^2 g^{-1}$	Unlisted	Unreported
Natural pumice [6]	Unlisted	8 $m^2 g^{-1}$	149 mmol kg^{-1}	Freundlich
Aluminum-coated pumice [6]	Unlisted	25 $m^2 g^{-1}$	195 mmol kg^{-1}	Freundlich
CuO nanoparticles [7]	Unlisted	89.6 $m^2 g^{-1}$	2.20 mmol kg^{-1}	Langmuir
Single-walled carbon nanotube [8]	Unlisted	400 $m^2 g^{-1}$	1.95 mmol kg^{-1}	Langmuir
Carboxylate group functionalized single-walled carbon nanotube [8]	Unlisted	400 $m^2 g^{-1}$	2.11 mmol kg^{-1}	Langmuir
Nano-scale zero-valent iron [10]	Unlisted	Unlisted	110 mmol kg^{-1}	Langmuir
Single-walled carbon nanotube [10]	Unlisted	400 $m^2 g^{-1}$	114 mmol kg^{-1}	Langmuir
Acid washed kaolinite [9]	Unlisted	14.7 $m^2 g^{-1}$	153 mmol kg^{-1}	Unlisted
Aluminia [9]	Unlisted	67.6 $m^2 g^{-1}$	248 mmol kg^{-1}	Unlisted
Fennel seed spent [27]	Unlisted	Unlisted	127 mmol kg^{-1}	Inconclusive
Rectorite [13]	410 $mmol_c kg^{-1}$	10 $m^2 g^{-1}$	400 mmol kg^{-1}	Langmuir
Ca-montmorillonite (SAz-2) [14]	1,300 $mmol_c kg^{-1}$	97 $m^2 g^{-1}$	1,500 mmol kg^{-1}	Langmuir
Na-montmorillonite (SWy-2) [14]	760 $mmol_c kg^{-1}$	32 $m^2 g^{-1}$	1,200 mmol kg^{-1}	Langmuir
Ca-montmorillonite (STx-1b) [14]	840 $mmol_c kg^{-1}$	84 $m^2 g^{-1}$	1,100 mmol kg^{-1}	Langmuir
Ca-montmorillonite (SAz-1) (this study)	1,230 $mmol_c kg^{-1}$	65 $m^2 g^{-1}$	1,276 mmol kg^{-1}	Langmuir
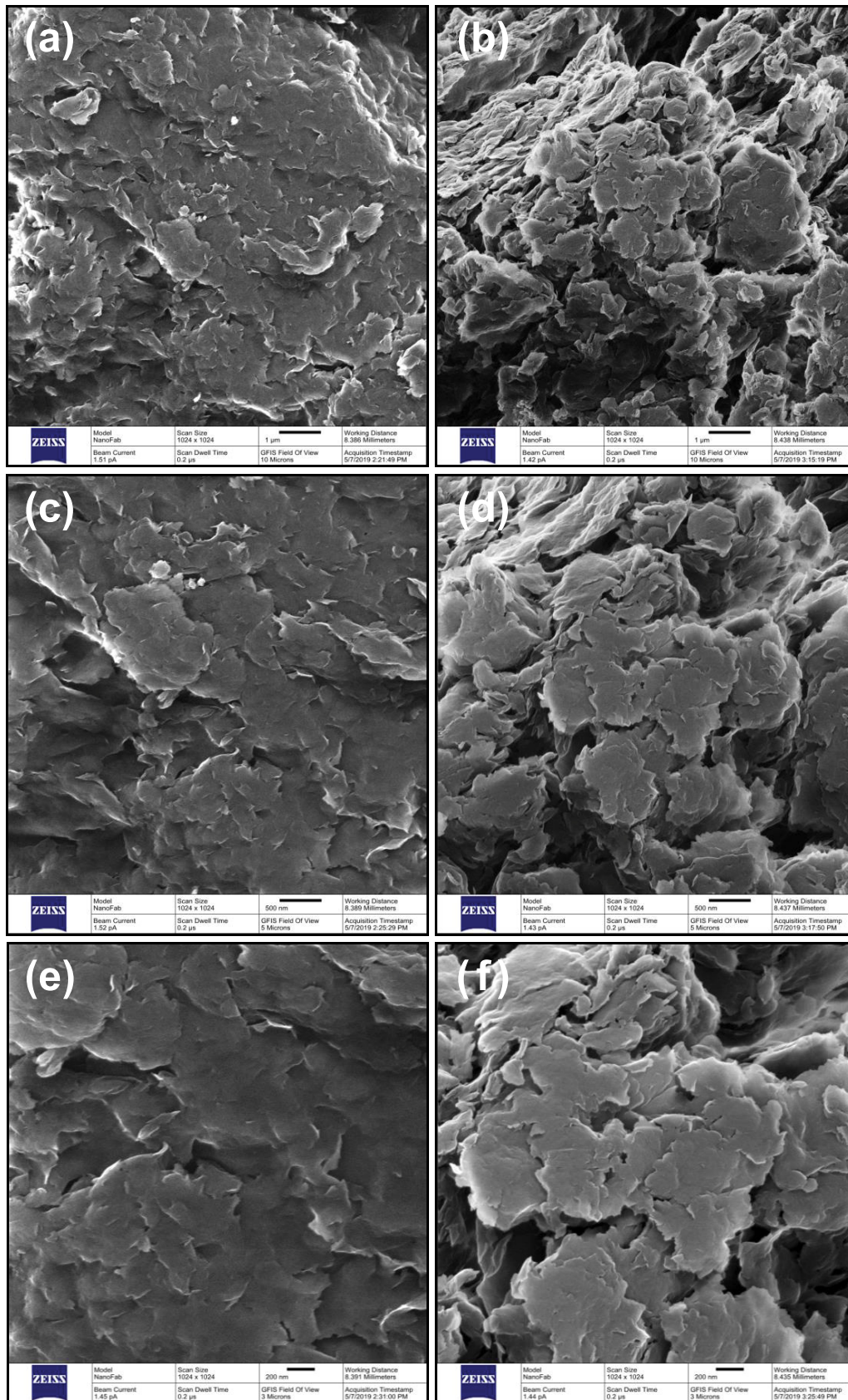
Fig. S2. Secondary electron images of raw SAz-1 (left) and SAz-1 loaded with ethidium bromide (right) at three different magnifications recorded with a helium ion microscope. The initial concentration was 14 mM.

Table S2
Adsorption kinetics for removal of ethidium bromide by some adsorbents

Adsorbent	Ethidium bromide ($mg\ L^{-1}$)	Adsorbent dose	pH	Temperature	Equilibrium time	Kinetic model
Graphene oxide [5]	0.5	0.5 mg/20 mL	8	298 K	17 min	Pseudo-second-order
Graphene oxide [26]	0.1–0.7	0.5 mg/20 mL	10	288–303 K	17 min	Pseudo-second-order
Natural pumice [6]	30, 100	8 g L^{-1}	8	298 K	3.5 h	Pseudo-second-order
Aluminum-coated pumice [6]	30, 100	8 g L^{-1}	8	298 K	3.5 h	Pseudo-second-order
CuO nanoparticles [7]	0.3	1.5 g L^{-1}	9	298–318 K	8 min	Pseudo-second-order
Single-walled carbon nanotube [8]	30	20 mg/20 mL	Unlisted	298 K	6 min	Intraparticle diffusion
Carboxylate-functionalized carbon nanotube [8]	30	20 mg/20 mL	Unlisted	298 K	6 min	Intraparticle diffusion
Nano-scale zero-valent iron [10]	20	30 mg/50 mL	Unlisted	293 K	5 min	Unlisted
Single-walled carbon nanotube [10]	20	30 mg/50 mL	Unlisted	293 K	5 min	Unlisted
Fennel seed spent [27]	5–20	50 mg/50 mL	Unlisted	298 K	15 min	Pseudo-second-order
Rectorite [13]	1,577	0.2 g/20 mL	8–9	303 K	~1 h	Pseudo-second-order
Ca-montmorillonite (SAz-2) [14]	3,943	1.0 g/100 mL	Unlisted	Unlisted	~1 h	Pseudo-second-order
Na-montmorillonite (SWy-2) [14]	3,943	1.0 g/100 mL	Unlisted	Unlisted	~1 h	Pseudo-second-order
Ca-montmorillonite (STx-1b) [14]	3,943	1.0 g/100 mL	Unlisted	Unlisted	~1 h	Pseudo-second-order
Ca-montmorillonite (SAz-1) (this study)	3,154	0.1 g/20 mL	7	303 K	~1 h	Pseudo-second-order